Neurosci. Bull.
https://doi.org/10.1007/s12264-024-01230-1

www.neurosci.cn
www.springer.com/12264

ORIGINAL ARTICLE

Modulation of Nicotine-Associated Behaviour in Rats By μ-Opioid Signals from the Medial Prefrontal Cortex to the Nucleus Accumbens Shell

Feng Zhu[1] · Hirosato Kanda[3] · Hiroyuki Neyama[4] · Yuping Wu[4] · Shigeki Kato[5] · Di Hu[4] · Shaoqi Duan[1] · Koichi Noguchi[1] · Yasuyoshi Watanabe[4] · Kazuto Kobayashi[5] · Yi Dai[1] · Yilong Cui[1,2,4]

Received: 1 November 2023 / Accepted: 8 January 2024

Abstract Nicotine addiction is a concern worldwide. Most mechanistic investigations are on nicotine substance dependence properties based on its pharmacological effects. However, no effective therapeutic treatment has been established. Nicotine addiction is reinforced by environments or habits. We demonstrate the neurobiological basis of the behavioural aspect of nicotine addiction. We utilized the conditioned place preference to establish nicotine-associated behavioural preferences (NABP) in rats. Brain-wide neuroimaging analysis revealed that the medial prefrontal cortex (mPFC) was activated and contributed to NABP. Chemogenetic manipulation of μ-opioid receptor positive (MOR^+) neurons in the mPFC or the excitatory outflow to the nucleus accumbens shell (NAcShell) modulated the NABP. Electrophysiological recording confirmed that the MOR^+ neurons directly regulate the mPFC-NAcShell circuit *via* $GABA_A$ receptors. Thus, the MOR^+ neurons in the mPFC modulate the formation of behavioural aspects of nicotine addiction *via* direct excitatory innervation to the NAcShell, which may provide new insight for the development of effective therapeutic strategies.

Keywords Nicotine-associated behaviour · μ-Opioid receptor · Medial prefrontal cortex · Nucleus accumbens shell · Small-animal neuroimaging

Introduction

Tobacco has been used for a long history as a recreational substance which can be traced back to ancient civilizations in the Americas [1]. Modern medical science clearly demonstrates that sustained tobacco use induces profound health hazards such as lung cancer, heart disease, and respiratory problems. The Global Burden of Disease Project estimated that the worldwide consumption of ~7.4 trillion cigarettes in 2019 led to ~7 million deaths [2]. However, its addictive nature makes it difficult for them to quit. The addictive nature of tobacco is believed to be primarily a result of the pharmacological effects of nicotine. Nicotine acts on nicotinic acetylcholine receptors (nAChRs) located in the brain, contributing to its addictive properties. Multiple pharmacological effects of nicotine have been reported and widely discussed as the substance dependence property of nicotine. For example, nicotine activates the mesolimbic dopaminergic system which is a critical reward system in the brain to produce euphoria, leading to reinforcement and sustaining nicotine intake [3]. On the other hand, nicotine addiction is reinforced by some conditioned habits or specific scenes without the direct pharmacological effect of nicotine, indicating the behavioural aspect of nicotine addiction [4–6]

Supplementary Information The online version contains supplementary material available at https://doi.org/10.1007/s12264-024-01230-1.

✉ Yi Dai
ydai@hyo-med.ac.jp

✉ Yilong Cui
cuiyl@riken.jp

1 Department of Anatomy and Neuroscience, Hyogo Medical University, Nishinomiya, Hyogo 663-8501, Japan

2 Laboratory for Brain-Gut Homeostasis, Hyogo Medical University, Nishinomiya, Hyogo 663-8501, Japan

3 School of Pharmacy, Hyogo Medical University, Kobe, Hyogo 650-8530, Japan

4 RIKEN Center for Biosystems Dynamics Research, Kobe, Hyogo 650-0047, Japan

5 Department of Molecular Genetics, Fukushima Medical University Institute of Biomedical Sciences, Fukushima 960-1295, Japan

Published online: 08 June 2024

which is similar to general behavioural addiction, such as gambling [7, 8] and binge-eating disorder [9]. However, whether and how the underlying neurobiological mechanisms of the behavioural aspect of nicotine addiction share nicotine substance addiction remains unclear.

Human neuroimaging studies have elucidated the hierarchical brain regions involved in nicotine-associated behaviour, including the prefrontal, insular, and anterior cingulate cortices, and subcortical areas [10–12]. A clinical intervention study showed that transient inactivation of the left dorsolateral prefrontal cortex using transcranial magnetic stimulation eliminates smoking craving behaviour [11]. However, the detailed neurobiological basis underlying the behavioural aspect of nicotine addiction remains elusive due to the lack of comparable animal studies that allow mechanistic investigation with molecular, cellular, and genetic manipulation. Several studies have established animal experimental paradigms to explore the behavioural aspect of nicotine addiction, such as the nicotine self-administration operant and conditioned place preference (CPP) paradigms. A growing number of studies have demonstrated that most neural activity and plastic changes in response to nicotine-related behaviour are observed in the reward- and memory-related regions, including the mesolimbic cortex, hippocampus, and amygdala, using physiological, pharmacological, and behavioural experiments [13–16]. However, most animal studies have been limited to the mesolimbic reward system and related brain areas. The behavioural aspect of nicotine addiction involves complicated brain functions, including cognition and execution, as well as reward and memory. Therefore, a brain-wide comparative exploration is necessary to reveal the comprehensive neural and molecular mechanisms of nicotine-associated behaviour.

Opioids and endogenous opioid systems are known to be involved in diverse addictive disorders, including behavioural addiction. Both synthetic and endogenous opioids have been demonstrated to interact with the mesolimbic dopaminergic system through their specific receptors, mostly *via* the μ-opioid receptor (MOR), to produce euphoria, leading to substance abuse [17–19]. Functional cross-interactions between opioids and nicotine have long been implicated in nicotine dependence due to the mechanistic overlap between opioids and nicotine in the mesolimbic dopaminergic system. Pharmacological studies have shown that endogenous μ-opioid signals modulate nicotine-induced dopamine increase in the nucleus accumbens (NAc), indicating its critical role in nicotine substance addiction [20]. Clinical studies have demonstrated that endogenous opioid systems are involved in nicotine-associated seeking behaviours. For instance, both intravenous naloxone administration and oral naltrexone administration have been reported to decrease smoking-seeking desire [21–23]. Despite accumulating clinical evidence, the underlying neurobiological basis of whether and how the endogenous opioid system modulates the behavioural aspect of nicotine addiction remains elusive.

To address this issue, we successfully established nicotine-associated behavioural preference in rats using the CPP paradigm and found that behavioural preference significantly increased after 3 days of conditioning with nicotine injection. In this animal model, we performed a brain-wide investigation to identify the primary regional brain activity in response to nicotine-associated behavioural preferences using a small-animal neuroimaging approach combining 2-deoxy-2-[^{18}F]fluoro-D-glucose (FDG) positron emission tomography (PET) imaging with voxel-based statistical parametric mapping analysis which allows for the analysis of rodent brain activity under conscious conditions [24–27]. Our brain-wide neuroimaging analysis revealed that regional brain activity was significantly increased in the medial prefrontal cortex (mPFC) and correlated with nicotine-associated behavioural preference. To further examine whether and how the endogenous opioid signal modulates such behavioural preference, we developed genetically engineered rats expressing Cre recombinase under the control of the MOR 1 (Oprm1) promoter [28], in which the neuronal activity of MOR$^+$ neurons can be specifically manipulated by optogenetic or chemogenetic methods. Our chemogenetic experiments clearly showed that MOR$^+$ neurons in the mPFC modulate the nicotine-associated behavioural preference *via* the excitatory projection into the Shell of NAc (NAcShell). Finally, our whole-cell patch-clamp recording clearly demonstrated that MOR$^+$ neurons in the mPFC directly inhibit excitatory outflow of the mPFC to the NAcShell *via* the $GABA_A$ receptor. Here we provide novel insight into the neurobiological basis of the behavioural aspect of nicotine addiction and demonstrate that MOR$^+$ neurons in the mPFC modulate the formation of the behavioural aspect of nicotine addiction through control of excitatory input into NAcShell that may contribute to alternative treatment for nicotine addiction.

Materials and Methods

All the experimental protocols were approved by the Institutional Animal Care and Use Committee of RIKEN (Kobe Branch, Japan). Animal experiments were performed according to the Principles of Laboratory Animal Care (National Institutes of Health, Publication No. 85-23, revised 2011). Behavioural studies were performed according to the Animal Research Reporting of *In Vivo* Experiments (ARRIVE) guidelines [29]. All efforts were made to minimize animal suffering and use.

Animal

All animals were housed at the temperature of 22 ± 1 °C, with 45% ± 15% humidity, and under a 12-h light and 12-h dark cycle. The rats were fed a standard pellet diet (Oriental Yeast Co., Tokyo, Japan) and provided with tap water *ad libitum*. Male 8-week-old Wistar rats (SLC, Shizuoka, Japan) were used. To chemogenetically manipulate the activity of MOR^+ neurons *in vivo*, we introduced male Long-Evans wild-type rats and male Long-Evans transgenic rats (MOR-Cre) which were described previously in detail [28].

Conditioned Place Preference (CPP)

The CPP was conducted using a three-compartment place-conditioning apparatus (ENV-013; Med Associates Inc., Fairfax, USA) with a distinct and tactile context. The black chamber had a grid-rod floor, whereas the white chamber had a mesh floor (length: 30.48 cm; width: 21 cm; height: 21 cm). The animal position and locomotor activity were automatically detected with infrared photobeams within the apparatus. This procedure was modified from previous studies [30, 31]. The CPP behavioural experiment was divided into four phases: habituation, baseline, conditioning, and testing.

During the habituation phase (days 1–2), the rats freely explored each chamber for 20 min. Habituation was conducted every half day, once in the morning, and once in the afternoon.

The CPP baseline was tested on the morning of day 3, during which the rats freely explored all the chambers with the partition gates open for 20 min. The chamber in which the rats spent the most time was defined as the preferred chamber; otherwise, it was defined as the non-preferred chamber. The CPP score of the pre-test was defined as the time spent in the non-preferred chamber divided by the total time spent in the two chambers [32]. After the CPP baseline test, the rats were randomly divided into each experimental group.

The conditioning phase was conducted from days 4 to 6. The rats received two conditioning sessions per day with at least a 4-h interval, one with a subcutaneous injection of saline in the morning and the other with a subcutaneous injection of nicotine in the afternoon. Nicotine hydrogen tartrate (Sigma-Aldrich, MA, USA, Cat #SML1236) was dissolved in saline. Different concentrations (0.3 mg/kg, 0.8 mg/kg, 1.2 mg/kg, and 1.5 mg/kg, s.c.) were used. Following saline or nicotine administration, the animals were confined to the non-preferred (paired with nicotine) or preferred (paired with saline) chamber, respectively, with the partition gate closed for 20 min.

The CPP test phase was conducted on day 7. The rats explored the three compartments freely for 20 min in a drug-free state. The CPP score was defined as the time spent in a nicotine-paired chamber (non-preferred chamber) divided by the total time spent in the two chambers [32]. The ΔCPP score is defined as the CPP score of the CPP test phase minus that of the pre-test phase. Rats were excluded based on predefined exclusion criteria (spending > 80% of their time in one chamber) [33].

In addition to the time spent in the chambers, the number of entries and locomotor activity were automatically detected. One entry is defined as the breaking of any beam beyond the first entry into a zone. An activity was defined as any beam breaking within the current zone. The devices were wiped with clean water after each rat was removed from the device and dried using a cloth.

For chemogenetic manipulation, designer receptors exclusively activated by the designer drug (DREADD) agonist CNO (clozapine N-oxide; Enzo Life Sciences, Tokyo, Japan, Cat #BML-NS105-0025) were intraperitoneally (1 mg/kg, i.p.) injected 1 h before the nicotine conditioning phase or test phase.

PET Scanning

All PET scans were conducted using a microPET Focus220 (Siemens Co., Ltd., Knoxville, USA) with a spatial resolution of 1.4 mm in full width at half maximum (FWHM) at the centre of the field of view, as previously reported [25, 34]. At least 1 h before ^{18}F-FDG injection, the rats underwent tail vein cannulation under 1.5% isoflurane anesthesia. The catheter was fixed to the tail using tape.

For PET scanning of the CPP baseline and test, the rats received an intravenous injection of ^{18}F-FDG (~70–75 MBq/0.4 mL) and were immediately placed in the CPP device for 20 min. Subsequently, the rats were returned to their respective cages. Forty-five min after ^{18}F-FDG intravenous injection, the rats were anesthetized with 1.5% isoflurane and placed in the gantry of a PET scanner. During the scan, a heating blanket was used to maintain body temperature at ~37 °C, and a thermocouple probe was inserted into the rectum to monitor body temperature. A 30-min emission scan was performed 55 min after the ^{18}F-FDG injection. The acquired emission data were collected in the three-dimensional-list mode and sorted into a single sinogram. The data were reconstructed using a standard two-dimensional filtered back projection (FBP) algorithm for quantitative evaluation or a statistical maximum a posteriori probability algorithm (MAP) for image co-registration.

Image Analysis

Voxel-based statistical analysis was performed according to previous reports [25, 34]. Briefly, using the PMOD software package (version 3.6, PMOD Technologies, Ltd.,

Zurich, Switzerland), individual MAP-reconstructed FDG images were co-registered to an FDG image template using a mutual information algorithm with Powell's convergence optimization method. The FDG templates were transformed into the space of the magnetic resonance imaging (MRI) reference template. The MRI reference template was placed in the Paxinos and Watson stereotactic spaces. Transformation parameters were obtained from individual MAP-reconstructed FDG images. These transformation parameters were applied to each FBP-reconstructed FDG image. To be consistent with the default parameter settings in the SPM software (Welcome Department of Imaging Neuroscience, London, UK), the voxel size of the template was scaled by a factor of 10. The final voxel size was resampled at 1.2 mm × 1.2 mm × 1.2 mm. Finally, to enhance statistical power, each FBP image was spatially smoothed using an isotropic Gaussian kernel (6-mm FWHM).

Voxel-based statistical analysis was performed using the SPM8 software (Wellcome Department of Imaging Neuroscience, London, UK). Global differences in FDG uptake were normalized to whole-brain uptake. A two-sample *t*-test was used to estimate the statistical differences between groups. The statistical threshold was set at $P < 0.005$ (uncorrected), with an extent threshold of 200 contiguous voxels.

Stereotaxic Surgery

For intracranial injection, glass micropipettes (Drummond Scientific, PA, USA) pulled using a puller (PP-83; Narishige Group, Tokyo, Japan) were used. We delivered AAV at a rate of 60 nL/min using an ultra-micropump (UMP3; World Precision Instruments, FL, USA) under 1.5% isoflurane anesthesia. The pipette was left for an additional 3 min after injection, to allow diffusion of the virus at the injection site and then slowly withdrawn, and then the skin incision was sutured. We injected penicillin (Meiji Seika, Tokyo, Japan) 200 μL to prevent postoperative infection after surgery. Three weeks after surgery, the rats were used for experiments.

All AAV vectors are listed in Table S2. To specific manipulation of the mPFC-NAcShell neural circuit, we first injected a mixture of AAVrg-hSyn-eGFP (85 nL) and AAVrg-pgk-Cre (215 nL) into the bilateral NAcShell of 8-week-old Wistar rats at stereotaxic coordinates from bregma: +2.16 mm anteroposterior (AP), ±1.0 mm mediolateral (ML), −7.2 mm dorsoventral (DV). One week later, 400 nL of AAV-hSyn-DIO-hM4D-mCherry were bilaterally injected into the mPFC (+3 mm AP, ±0.65 mm ML, 3.6 mm DV). For specific activation of MOR^+ neurons in the mPFC, 400 nL of AAV-hSyn-DIO-hM3D-mCherry were bilaterally injected into layer 5 of the mPFC (+3 mm and 3.24 mm AP, ±0.65 mm ML, 3.6 mm DV) of 7-week-old MOR-Cre rats.

For the whole-cell patch-clamp recording, 300 nL of AAVrg-hSyn-eGFP were bilaterally injected into the NAcShell (+2.16 mm AP, ±1.0 mm ML, −7.2 mm DV) of 5 weeks MOR-Cre rats with 400 nL AAV-EF1a-Flex-hChR2(H134R)-mCherry were bilateral injected into layer 5 of the mPFC (+3 mm and 3.24 mm AP, ±0.65 mm ML, 3.6 mm DV) in the next day after the NAcShell injection.

Immunohistochemistry

The rats were transcranially perfused with PBS under deep isoflurane anesthesia, followed by 4% paraformaldehyde (PFA; Nacalai, Osaka, Japan) in PBS. Then the brain was removed and soaked in 4% PFA to postfix overnight at 4 °C. The brain tissues were then transferred to 30% sucrose for 2 days. Serial brain sections were cut at 30 μm thickness using a cryostat (Cryostar NX70, Epredia Holdings Ltd., NH, USA) and collected in dishes containing PBS with 0.05% Sodium Azide (FUJIFILM Wako Pure Chemical Corporation, Osaka, Japan). To confirm the AAV injection, brain sections were mounted onto coated glass slides and directly observed without immunostaining.

Fluorescent images were acquired using a Zeiss LSM 710 confocal microscope (Carl Zeiss, Oberkochen, Germany) and analyzed using ZEN software (Carl Zeiss).

Brain Slice Preparation

After AAV injection, the MOR-Cre rats were deeply anesthetized with isoflurane and decapitated. In brief, the whole brain was rapidly dissected out and coronal brain slices (400 μm), containing mPFC and NAcShell, were made with a vibratome (VT1200, Leica, Wetzlar, Germany). Slices were submerged in a normal Krebs solution that contained (in mmol/L):117 NaCl, 3.5 KCl, 2.5 $CaCl_2$, 1.2 $MgCl_2$, 1.2 NaH_2PO_4, 25 $NaHCO_3$, 11 glucose, and osmolarity of 324 mOsm. The Krebs solution was saturated with 95% O_2 and 5% CO_2 and had a pH of 7.35 at room temperature of 24 °C. The brain slice was then fixed in a recording chamber with a slice anchor. The chamber was mounted on the stage of an Olympus IX50 microscope (Olympus, Tokyo, Japan) which was equipped with infrared differential interference contrast (IR-DIC) and fluorescent imaging systems.

Whole-Cell Patch-Clamp Recording

$eGFP^+$ or $mCherry^+$ neurons were first identified under epifluorescence illumination in the mPFC, located from Bregma +3.0 mm to +2.52 mm. Under the IR-DIC microscope, whole-cell patch-clamp recordings were performed on the mPFC neurons labelled with fluorescent proteins. The electrode resistance after filling the recording electrode internal solution ranged from 3 to 5 MΩ. For the voltage-clamp

experiment, recording pipettes were filled with a solution containing (in mmol/L): 135 $CsMeSO_3$, 5 CsCl, 0.5 $CaCl_2$, 2.4 $MgCl_2$, 5 EGTA, 10 HEPES, 5 Na_2ATP, 0.33 GTP-TRIS salt and 2 QX-314; the pH of the solution was adjusted to 7.35 with CsOH. In a current-clamp experiment, 135 K-gluconate, 5 KCl, 0.5 $CaCl_2$, 2.4 $MgCl_2$, 5 EGTA, 10 HEPES, 5 Na_2ATP, 0.33 GTP-TRIS salt were used; the pH of the solution was adjusted to 7.35 with KOH. After establishing the whole-cell configuration, the cells were held at −60 mV and $GABA_A$ receptor-mediated inhibitory currents were measured at +10 mV. ChR2-expressing MOR^+ neurons were activated by 470 nm LED light (Thorlabs, Newton, USA). The blue light was applied through an objective (×40, water immersion objective), and the light intensity was controlled using a light controller unit (Thorlabs). Signals from voltage-clamp experiments were amplified using an Axopach 200 B amplifier, filtered at 2 kHz, and sampled at 10 kHz using pCLAMP 10 software (Molecular Devices, Sunnyvale, USA).

Statistical Analysis

All data were calculated using Graphpad Prism version 9 (Graphpad Software, San Diego, USA) and shown as the mean ± SEM. Two-way analysis of variance (ANOVA) followed by Sidak's multiple comparison test and paired *t*-test were used. Pearson's test was used for correlation analysis. The significance threshold was placed at $*P<0.05$, $**P<0.01$, and $***P<0.001$.

Data Availability

The data supporting the findings of this study are available from the corresponding author upon reasonable request.

Results

Nicotine-associated Behavioural Preference Established by the CPP Paradigm

The CPP behavioural paradigm has been used extensively to assess behavioural preferences. Thus, we used it to evaluate nicotine-associated behavioural preferences (Fig. 1A). During habituation, the rats gradually acclimated to the CPP device, and their side preference became stable. The pre-conditioning baseline side preference was assessed after four habituation sessions, and no significant difference was observed between the experimental groups (Fig. 1B). To examine the dose-dependent response to nicotine, rats were conditioned with 0, 0.3, 0.8, or 1.5 mg/kg nicotine for 3 days (Fig. 1B) ($n=6$ in each group). The side preference was significantly affected by the concentration factor ($F_{(3, 20)}=6.572$, $P=0.0029$), and increased in the rats conditioned with 0.8 mg/kg ($P=0.0101$) and 1.5 mg/kg ($P=0.0403$) nicotine. Interestingly, the side preference at a higher dose (1.5 mg/kg) slightly decreased, as previously reported [35]. Given the higher CPP score during the CPP test phase, we chose 0.8 mg/kg for the next experiments.

To investigate the nicotine conditioning-induced behavioural characteristics, we further analyzed the time spent, the number of entries, and locomotor activity in each chamber before (pre-test) and after (test) nicotine conditioning. In the vehicle group ($n=6$), the time spent (phase factor: $F_{(1, 10)}=0.4032$, $P=0.5397$), number of entries (phase factor: $F_{(1, 5)}=0.0001$, $P=0.9920$), and locomotor activity (phase factor: $F_{(1, 5)}=0.1134$, $P=0.7499$) in the non-preferred chamber were not changed (time spent: $P=0.5561$, number of entries*:* $P=0.6742$, locomotor activity: $P=0.9990$) by the conditioning procedure when compared pre-test and test phase and the balance of these behavioural properties between preferred and non-preferred chambers remained almost unchanged, except for the number of entries (treatment factor: $F_{(1, 5)}=4.089$, $P=0.0991$; $P=0.0396$ when compared preferred chamber and non-preferred chamber during pre-test phase, $P=0.8354$ during the test phase) (Fig. 1C–E). In contrast, the time spent (phase × treatment factor: $F_{(1, 10)}=23.28$. $P=0.0007$) and locomotor activity (phase factor: $F_{(1, 5)}=17.63$, $P=0.0085$) were significantly increased (time spent: $P=0.0014$, locomotor activity: $P=0.0054$) in the nicotine-paired chamber after conditioning with 0.8 mg/kg nicotine (Fig. 1F, H) ($n=6$). Meanwhile, the number of entries in both chambers (phase factor: $F_{(1, 5)}=19.27$, $P=0.0071$) was significantly increased (preferred chamber: $P=0.014$, non-preferred chamber: $P=0.0105$) after conditioning with 0.8 mg/kg nicotine (Fig. 1G), indicating an increased exploratory activity in these rats. These results indicated that both behavioural preferences and exploratory activity were induced by nicotine conditioning.

Finally, we analyzed the locomotor activity during the conditioning phase. In the vehicle group, the locomotor activity after vehicle injection (day × treatment factor: $F_{(2, 20)}=0.6152$, $P=0.5504$) showed decreased tendency during conditioning phase, probably due to the adaptive effect on the chambers (Fig. 1I). Whereas the locomotor activity after nicotine injection (day × treatment factor: $F_{(2, 20)}=11.30$, $P=0.0005$) significantly increased in day 5 ($P=0.0013$) and day 6 ($P=0.0049$) as compared with day 4 in the nicotine 0.8 mg/kg group (Fig. 1J). This result is consistent with the evidence that nicotine exposure induces hyper-locomotor activities [36, 37].

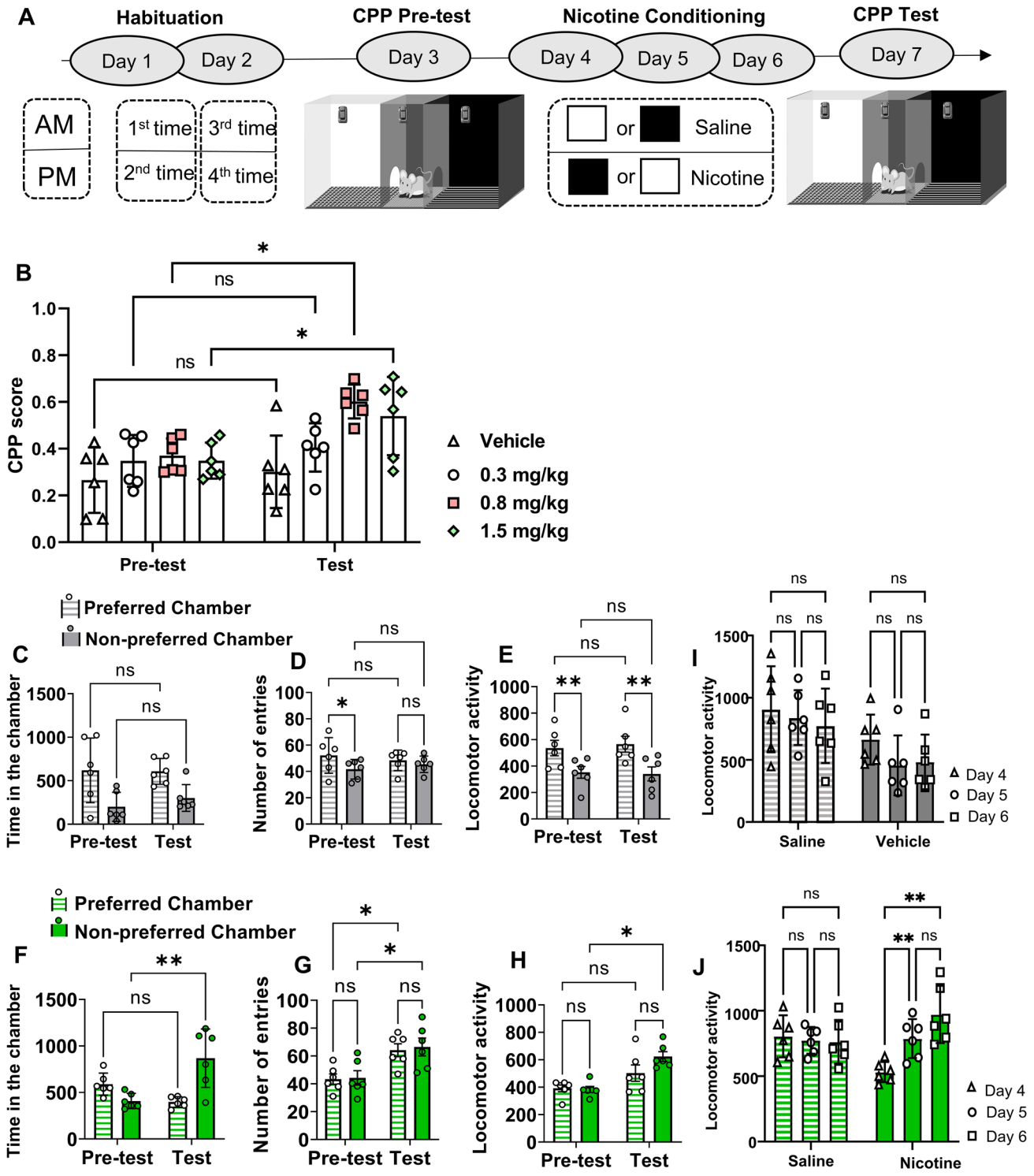

Fig. 1 Nicotine-associated behavioural preference evaluated by CPP paradigm. **A** Experimental design of CPP. The white square means white chamber and the black square means black chamber. They are paired with nicotine or saline injection. **B** CPP score in saline ($n=6$), nicotine 0.3 mg/kg ($n=6$), nicotine 0.8 mg/kg ($n=6$), and nicotine 1.5 mg/kg ($n=6$) groups. **C–E** Time spent (**C**), the number of entries (**D**), and locomotor activity (**E**) in the preferred chamber and non-preferred chamber during the pre-test and test phases of the saline group. **F–H** Time spent (**F**), the number of entries (**G**), and locomotor activity (**H**) in the preferred chamber and non-preferred chamber during the pre-test and test phases of the nicotine (0.8 mg/kg) group. **I, J** Locomotor activity post saline and post vehicle or nicotine injection during CPP conditioning phase in the vehicle group (**I**) and nicotine 0.8 mg/kg group (**J**). Two-way ANOVA with Sidak's multiple comparisons test (the mean ± SEM, $^{*}P<0.05$, $^{**}P<0.01$). ns: not significant. ANOVA, analysis of variance; CPP, conditioned place preference

Activation of the mPFC by Nicotine-associated Behavioural Preference

To examine brain-wide regional brain activity in response to nicotine-associated behavioural preference, we conducted an FDG-PET scan and subsequent voxel-based statistical analyses (Fig. 2A). Regional brain activity in response to nicotine-associated behavioural preference was assessed by comparing the brain-wide FDG uptake in the nicotine-conditioned ($n=14$, 0.8 mg/kg) group with that in the saline-conditioned ($n=7$) group. The nicotine-conditioned group showed significantly higher CPP scores during the test

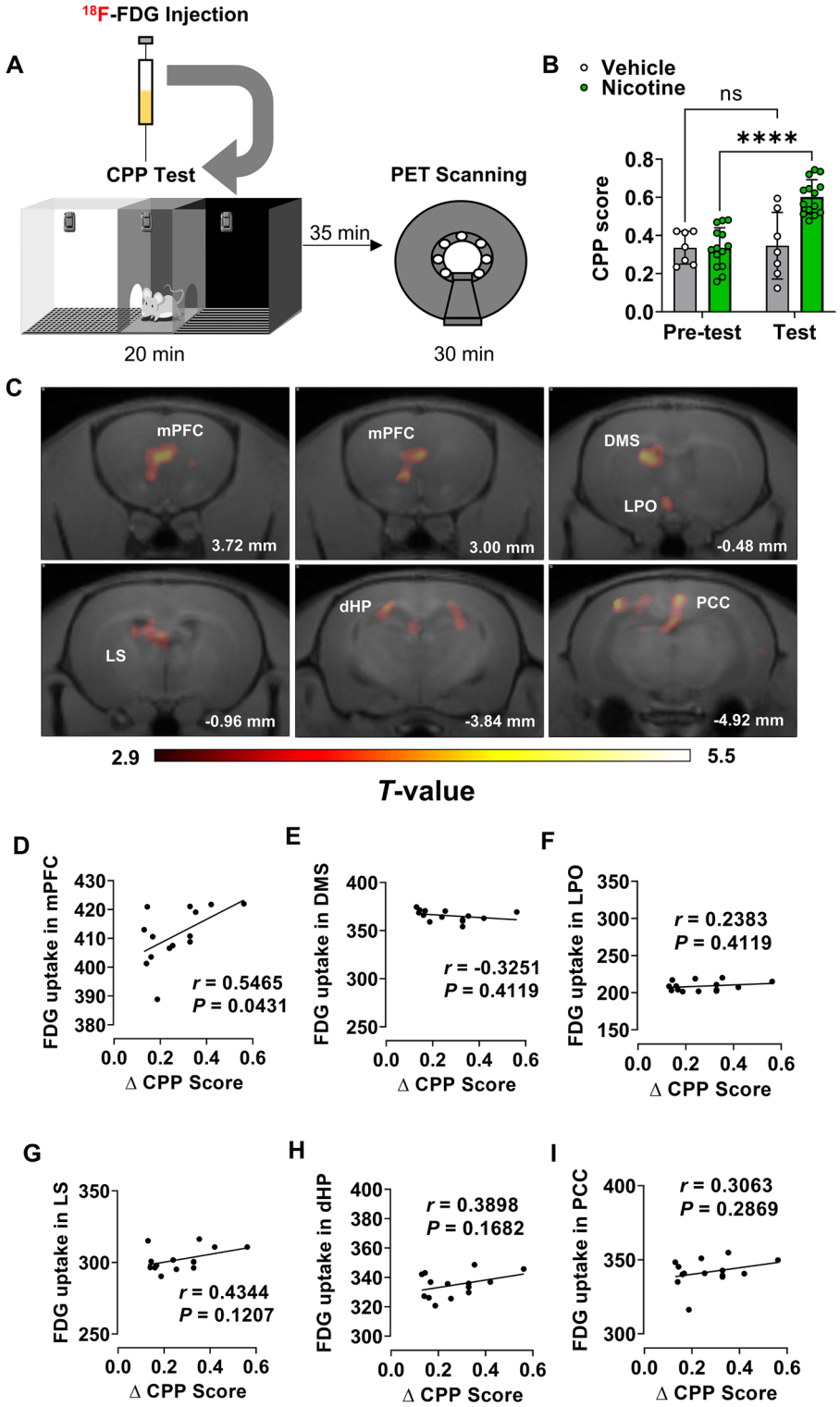

Fig. 2 Brain activity in response to nicotine-associated behavioural preference. **A** Experimental design of PET scanning. **B** CPP score of rats undergoing PET scanning ($n=7$ in vehicle group, $n=14$ in nicotine group), two-way ANOVA with Sidak's multiple comparisons test (the mean ± SEM, ****$P<0.0001$). **C** Brain activity in response to nicotine-associated behavioural preference. Images showing activated (red) brain regions during the CPP test phase ($n=14$). Images were obtained by voxel-based statistical comparison of FDG uptake with that of the CPP baseline phase. A T-value of 2.86 was used as the threshold corresponding to $P=0.005$ (uncorrected). The right side of the image indicates the left hemisphere. The number in the lower line indicates the level of coronal slices in the rat brain atlas (Paxinos and Watson). **D–I** Correlation between ΔCPP score and FDG uptake in mPFC ($P=0.0431$) (**D**), DMS ($P=0.4119$) (**E**), LPO ($P=0.4119$) (**F**), LS ($P=0.1207$) (**G**), dHP ($P=0.1682$) (**H**), and PCC ($P=0.2869$) (**I**). Person correlation analysis test. ANOVA, analysis of variance; CPP, conditioned place preference; dHP, dorsal hippocampus; DMS, dorsomedial striatum; FDG, 2-deoxy-2-[^{18}F] fluoro-D-glucose; LPO, lateral preoptic area; LS, lateral septal nucleus; mPFC, medial prefrontal cortex. PCC, posterior cingulate cortex; PET, positron emission tomography

phase (Fig. 2B) (phase factor: $F_{(1, 19)} = 19.77$, $P = 0.0003$; $P < 0.0001$ when comparing pre-test and test). Voxel-based statistical analysis revealed characteristic activation in several brain regions in response to nicotine-associated behavioural preferences, including the mPFC, dorsal medial striatum (DMS), lateral preoptic area (LPO), lateral septal nucleus (LS), dorsal hippocampus (dHP), and posterior cingulate cortex (PCC) (Fig. 2C, Table 1). To further assess the functional role of these activated regions in nicotine-associated behavioural preference, we analyzed the correlation between regional FDG uptake in these regions and the changes in behavioural preference (ΔCPP Score) (Fig. 2D–J). Interestingly, only FDG uptake in the mPFC was positively correlated with the ΔCPP Score (Fig. 2D) ($P = 0.0431$), indicating that the mPFC may contribute to nicotine-associated behavioural preference.

μ-Opioid Receptors in the mPFC Modulate Nicotine-associated Behavioural Preference

We then focused on the MOR in the mPFC since clinical studies have reported endogenous μ-opioid signals modulate nicotine-associated craving behaviour [38]. Accordingly, we also confirmed that nicotine-associated behavioural preference in the CPP test was significantly inhibited by the subcutaneous injection of naloxone (1 mg/kg), a MOR antagonist, 10 min before the nicotine conditioning or test phase (Fig. S2A, B). To further reveal whether and how endogenous μ-opioid signals in the mPFC are involved in nicotine-associated behavioural preference, we chemogenetically manipulated the MOR^+ neurons in the mPFC using genetically engineered rats expressing Cre recombinase under the control of the MOR promoter (MOR-Cre rats) [25]. In these MOR-Cre rats, we injected adeno-associated virus (AAV) (AAV-hSyn-DIO-hM3D-mCherry or AAV-hSyn-DIO-mCherry) into bilateral layer 5 of the mPFC, which is the major excitatory outflow region of the mPFC (hM3D group or control group, respectively) (Fig. 3B). Consistent with our previous report [28], immunofluorescence images showed that mCherry-positive neurons were scattered around layer 5 of the mPFC and in layers 2/3, indicating Cre-dependent recombination of these transgenes in MOR-Cre rats (Fig. 3B).

To examine the functional role of MOR^+ neurons in the mPFC on nicotine-associated behavioural preference, we first confirmed the dose-dependent response of nicotine for the CPP test in Long-Evans rats, which is the genetic background strain of MOR-Cre rats and found that 1.5 mg/kg nicotine was more appropriate to induce nicotine-associated behavioural preference ($n = 5$, $P = 0.0104$) in Long-Evans strain rats (phase × concentration factor, $F_{(2, 12)} = 4.155$ $P = 0.0425$) (Fig. 3A). Then, we chemogenetically manipulated MOR^+ neurons in the mPFC during the nicotine conditioning phase for consecutive 3 days (Fig. 3C) to explore the involvement of MOR^+ neurons in the formation of nicotine-associated behavioural preference. As shown in Fig. 3D, the nicotine-associated side preference (phase × treatment factor: $F_{(1, 13)} = 8.243$, $P = 0.0131$) was significantly increased in the control (mCherry, green bar) group ($n = 5$, $P = 0.0435$), in which CNO (1 mg/kg) was intraperitoneally injected 1 h before each nicotine injection for 3 consecutive days. In contrast, the increment of nicotine-associated side preference in the rats expressing hM3D (red bar) was completely analogously abolished by CNO treatment ($n = 10$, $P = 0.3885$), indicating the chemogenetic activation of MOR^+ neurons in the mPFC suppressed nicotine-associated behavioural preference (Fig. 3D). Similarly, the increment in the time spent (phase factor: $F_{(1, 18)} = 2.061$, $P = 0.1683$), the number of entries (phase factor: $F_{(1, 9)} = 2.795$, $P = 0.1289$), and locomotor activity (phase factor: $F_{(1, 9)} = 3.093$, $P = 0.1125$) in nicotine-paired chamber (non-preferred chamber) during CPP test phase were attenuated by chemogenetic activation of MOR^+ neurons in the mPFC during the conditioning phase (Fig. 3E–G). (time spent: $P = 0.1011$, number of entries: $P = 0.0092$, locomotor activity: $P = 0.7893$). Whereas the increased locomotor activity due to the direct pharmacological effect of nicotine was not changed after chemogenetic activation of MOR^+ neurons in the mPFC during the nicotine conditioning phase (Fig. 3H) (day × treatment factor: $F_{(2, 36)} = 10.24$, $P = 0.0003$; $P = 0.0074$ when comparing day 6 with day 4). These results suggested that chemogenetic activation of MOR^+ neurons in the mPFC

Table 1 Activated brain regions in response to nicotine-associated behavioural preference

Brain regions	Laterality	*T* value (peak)	Volume (mm^3)
Medial Prefrontal Cortex, mPFC	R	3.93	3.34
Dorsal medium straitum, DMS	R	4.54	1.62
Lateral preoptic area, LPO	R	4.07	0.36
Lateral septal nucleus, LS	R	3.89	1.46
Dorsal Hippocampus, dHP	L&R	4.42	7.99
Posterior Cingulate Cortex, PCC	L&R	4.03	1.69

Nicotine group ($n = 14$) *versus* vehicle group ($n = 7$), Heigh threshold: $T = 2.86$ with an extent threshold of 200 contiguous voxels, $P < 0.005$ uncorrected. L and R indicate the left and right hemispheres, respectively

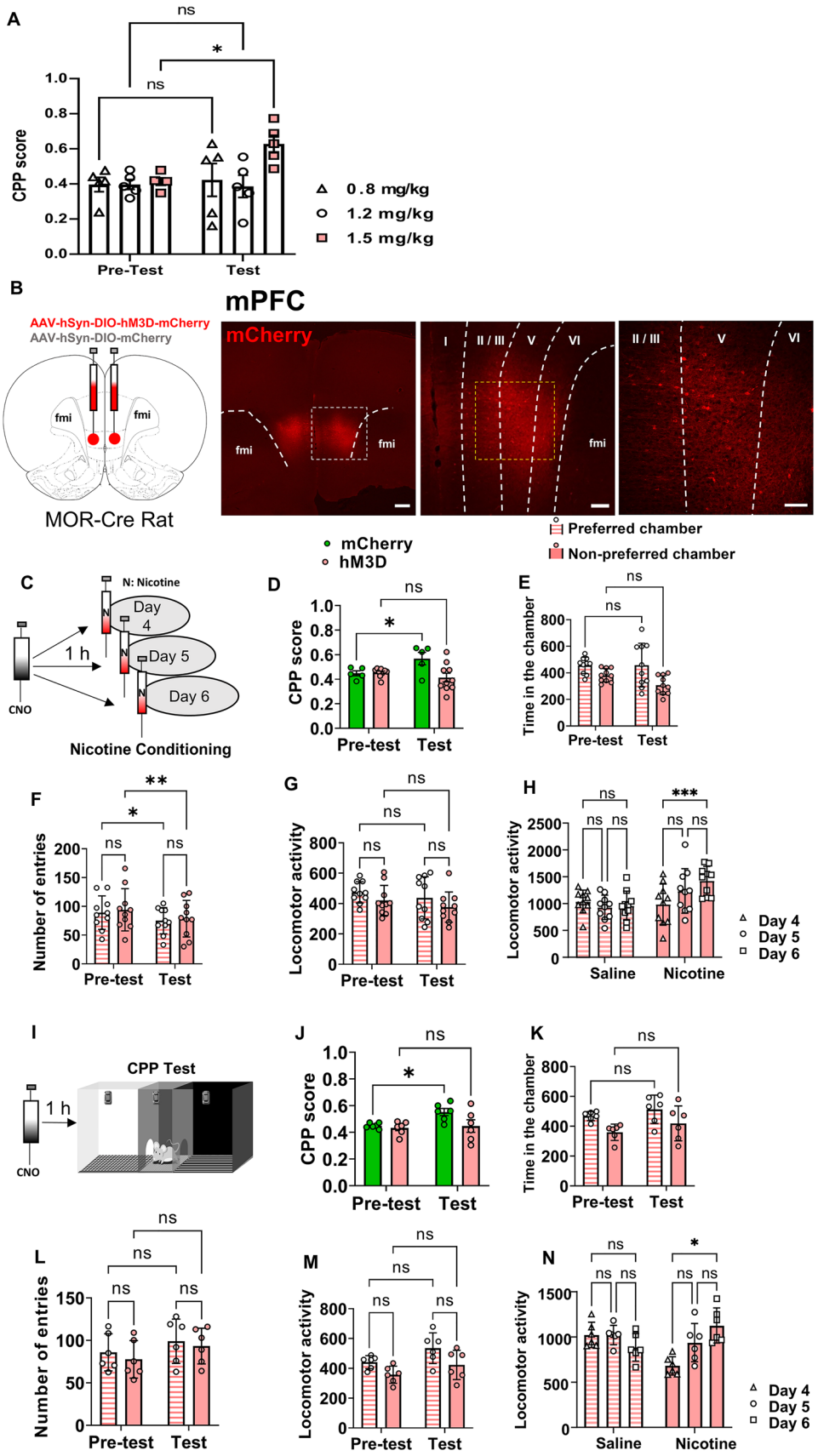

Fig. 3 μ-Opioid receptors in mPFC moderate nicotine-associated behavioural preference. **A** CPP score in nicotine 0.8 mg/kg ($n=5$), 1.2 mg/kg ($n=5$), and 1.5 mg/kg groups ($n=5$) of Long-Evans wild-type male rats. **B** Left: schematic diagram of injection of the virus (AAV-hSyn-DIO-hM3D-mCherry or AAV-hSyn-DIO-mCherry) in the mPFC of MOR-Cre rats. Right: representative images of mCherry (red) expression in mPFC neurons, scale bar, 500 μm. The imaging is enlarged by scale bars of 200 μm and 100 μm, respectively. **C** Schematic diagram of the CNO injection 1 h before the CPP conditioning phase on three consecutive days (days 4, 5, and 6). **D** CPP score in mCherry and hM3D-mCherry group with CNO injection 1 h before CPP conditioning phase. **E–G** Time spent (**E**), the number of entries (**F**), and locomotor activity (**G**) in the preferred chamber and non-preferred chamber during the pre-test and test phases of the hM3D group. **H** Locomotor activity post saline and post nicotine injection during CPP conditioning phase of hM3D group. **I** Schematic diagram of the CNO injection 1 h before the CPP test phase**. J** CPP score in mCherry and hM3D groups with CNO injection 1 h before the CPP test phase. **K–N** Time spent (**K**), the number of entries (**I**) and locomotor activity (**M**) in the preferred chamber and non-preferred chamber during the pre-test and test phases of the hM3D group. **N** locomotor activity post saline and post nicotine injection during CPP conditioning phase of hM3D group. Two-way ANOVA with Sidak's multiple comparisons test (the mean ± SEM. $^{**}P<0.01$, $^{*}P<0.05$). ns: not significant. ANOVA, analysis of variance; CNO, clozapine N-oxide, CPP, conditioned place preference; MOR, μ-opioid receptor; mPFC, medial prefrontal cortex

during the conditioning phase suppressed the formation of nicotine-associated behavioural preference and exploratory activity, but not the nicotine pharmacological effect itself.

Subsequently, we confirmed whether chemogenetic activation of MOR^+ neurons in the mPFC during the test phase modulates established nicotine-associated behavioural preference or not (Fig. 3I). As shown in Fig. 3J, the nicotine-associated side preference (phase factor: $F_{(1, 10)}=5.239$, $P=0.0451$) was significantly increased in the control (mCherry, green bar) group ($n=6$, $P=0.0348$) but not in the hM3D (red bar) group ($n=6$, $P=0.9100$). Accordingly, the increment in the time spent (phase factor: $F_{(1, 10)}=2.986$, $P=0.1147$), the number of entries (phase factor: $F_{(1, 5)}=4.307$, $P=0.0926$), and locomotor activity (phase factor: $F_{(1, 5)}=23.6$, $P=0.0046$) in nicotine-paired chamber (non-preferred chamber) during CPP test phase were inhibited by chemogenetic activation of MOR^+ neurons during CPP test phase (Fig. 3K–M) (time spent: $P=0.3509$, number of entries: $P=0.2270$, locomotor activity: $P=0.8348$). Similar to Fig. 3H nicotine pharmacological effect-evoked hyperactivity (day × treatment factor: $F_{(2, 20)}=14.77$, $P=0.0001$) was not affected by chemogenetic manipulation (Fig. 3N). ($P=0.0208$ when compared to days 6 and 4).

Chemogenetic activation of MOR^+ neurons in the mPFC either during formation or after the establishment of nicotine conditioning suppressed the behavioural aspect of nicotine addiction without affecting the direct pharmacological effect of nicotine.

The mPFC to NAcShell Circuit Is Indispensable for Nicotine-associated Behavioural Preference

Next, we examined the terminal field of the mPFC excitatory outflow to modulate the behavioural aspect of nicotine addiction. Because the NAcShell is known to receive abundant excitatory projections from the infralimbic cortex of the mPFC [39] and plays a critical role in rewarding processes and nicotine self-administration behaviour [40], we focused on the mPFC-NAcShell circuit to investigate whether and how the circuit modulates nicotine-associated behavioural preference. To specifically manipulate the mPFC-NAcShell circuit, we concomitantly injected a mixture of retrograde AAV (AAVrg)-hSyn-eGFP and AAVrg-pgk-Cre into the bilateral NAcShell, and AAV-hSyn-DIO-hM4D-mCherry or AAV-hSyn-DIO-mCherry (hM4D group or control group, respectively) into bilateral layer 5 of the mPFC in wild-type Wistar rats (Fig. 4A). Thus, immunofluorescence images showed that mCherry was specifically expressed in the $eGFP^+$ layer 5 projection neurons in the mPFC that send monosynaptic projection into the NAcShell. The eGFP was also seen in the injection area of the NAcShell (Fig. 4B).

To investigate the functional role of the mPFC-NAcShell circuit in nicotine-associated behavioural preferences, we first specifically suppressed circuit activity by chemogenetic manipulation during the conditioning phase. Consistently, the nicotine-associated side preference (phase × treatment factor: $F_{(1, 9)}=13.30$, $P=0.0053$) was significantly increased in the control (mCherry, green bar) group (Fig. 4D) ($n=6$, $P=0.0473$) following consecutive CNO injection (i.p., 1mg/kg, 1 h before each nicotine injection) for 3 days (Fig. 4C). However, the increase in the nicotine-associated side preference in the hM4D (red bar) group was completely reduced by CNO treatment (Fig. 4D) ($n=5$, $P=0.0708$). Likewise, the increments in the time spent (phase factor: $F_{(1, 8)}=0.02341$, $P=0.8822$), the number of entries (phase factor: $F_{(1, 4)}=12.41$, $P=0.0244$), and locomotor activity (phase factor: $F_{(1, 4)}=0.7407$, $P=0.4380$) in the nicotine-paired chamber (non-preferred chamber) of the CPP test were attenuated by the chemogenetic inhibition of the mPFC-NAcShell circuit during the conditioning phase (Fig. 4E–G) (time spent: $P=0.3440$, number of entries: $P=0.0346$, locomotor activity: $P=0.2907$). However, such specific manipulation of the mPFC-NAcShell circuit activity during the nicotine conditioning phase did not affect the increased locomotor activity (day factor: $F_{(1, 8)}=10.11$, $P=0.0130$) due to the direct pharmacological effect of nicotine (Fig. 4H) ($P=0.0454$ when compared day 6 and day 4). These results indicate that the mPFC-NAcShell circuit takes part in the formation of nicotine-associated behavioural preferences, but not in the pharmacological effect of nicotine.

Subsequently, we investigated whether chemogenetic inhibition of the mPFC-NAcShell circuit during the CPP test phase disturbed nicotine-associated behavioural preferences (Fig. 4I). As shown in Fig. 4J, the nicotine-associated side preference (phase factor: $F_{(1, 8)}=7.279$, $P=0.0272$) was significantly increased in the control (mCherry, green bar) group ($n=5$, $P=0.0073$) but not in the hM4D (red bar) group ($n=5$, $P=0.9670$). Consistently, the chemogenetic inhibition of the circuit during the CPP test phase attenuated the increase in the time spent (phase factor: $F_{(1, 8)}=0.6177$, $P=0.4545$), the number of entries (phase factor: $F_{(1, 4)}=4.728$, $P=0.0953$), and locomotor activity (phase factor: $F_{(1, 4)}=7.912$, $P=0.0482$) in the nicotine-paired chamber (non-preferred chamber) during the CPP test phase (Fig. 4K–M) (time spent: $P=0.9868$, number of entries: $P=0.9429$, and locomotor activity: $P=0.9769$). Moreover, the nicotine pharmacological effect-evoked hyperactivity (day × treatment factor: $F_{(2, 16)}=27.81$, $P<0.0001$) was not affected by the specific inhibition of the mPFC-NAcShell circuit (Fig. 4N) ($P=0.0079$ when comparing day 5 and day 4; $P=0.0005$ when comparing day 6 with day 4).

Overall, chemogenetic suppression of the mPFC-NAcShell circuit inhibited the formation and retention of the

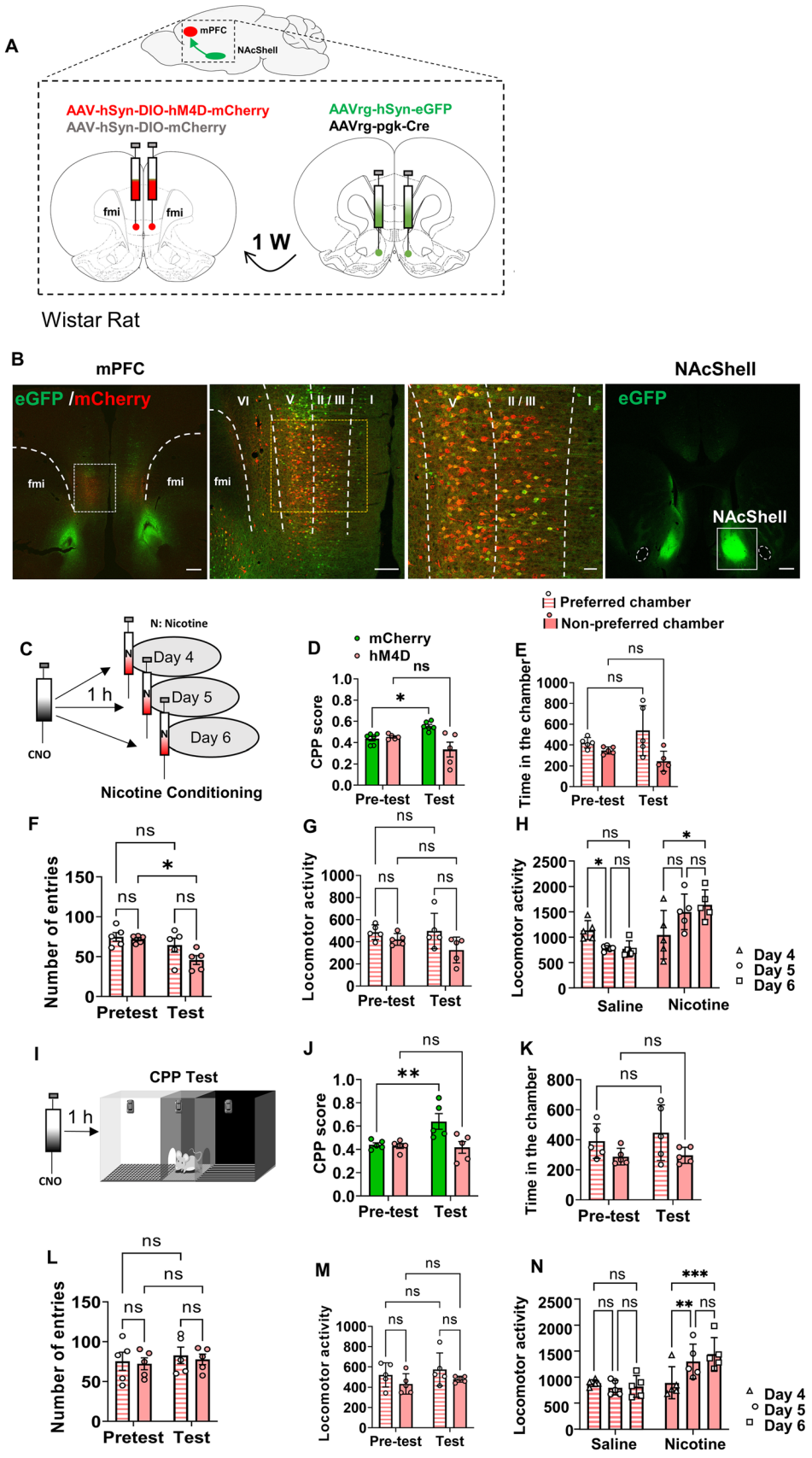

Fig. 4 mPFC–NAcShell circuit takes part in nicotine-associated behavioural preference. **A** Schematic diagram of the injection of virus (mixture of AAVrg-pgk-Cre and AAVrg-hSyn-eGFP) into the NAcShell and injection of virus (AAV-hSyn-DIO-hM4D-mCherry or AAV-hSyn-DIO-mCherry) into the mPFC of the Wistar wild-type rat after one week. **B** Representative images of double expression (yellow) of eGFP (green) and mCherry (red) in the mPFC regions, scale bar, 500 μm. The imaging is enlarged by scale bars of 200 μm and 50 μm respectively. The expression of eGFP in NAcShell is also seen (green), scale bar, 500 μm. **C** Schematic diagram of the CNO injection 1 h before the CPP conditioning phase on three consecutive days (days 4, 5, and 6)**. D** CPP score in mCherry and hM4D-mCherry group with CNO injection 1 h before CPP conditioning phase. **E–G** Time spent (**E**), the number of entries (**F**) and locomotor activity (**G**) in the preferred chamber and non-preferred chamber during the pre-test and test phases of the hM4D group. **H** Locomotor activity post saline and post nicotine injection during CPP conditioning phase of hM4D group. **I** Schematic diagram of the CNO injection 1 h before the CPP test phase**. J** CPP score in mCherry and hM4D group with CNO injection 1 h before CPP test phase. **K–M** Time spent (**K**), the number of entries (**I**), and locomotor activity (**M**) in the preferred chamber and non-preferred chamber during the pre-test and test phases of the hM4D group. **N** Locomotor activity post saline and post nicotine injection during CPP conditioning phase of hM4D group. Two-way ANOVA with Sidak's multiple comparisons test (the mean ± SEM. $^{***}P<0.001$, $^{**}P<0.01$, $^{*}P<0.05$). ns, not significant. ANOVA, analysis of variance; CNO, clozapine N-oxide; CPP, conditioned place preference; eGFP, enhanced green fluorescent protein; NAcShell, shell of nucleus accumbens

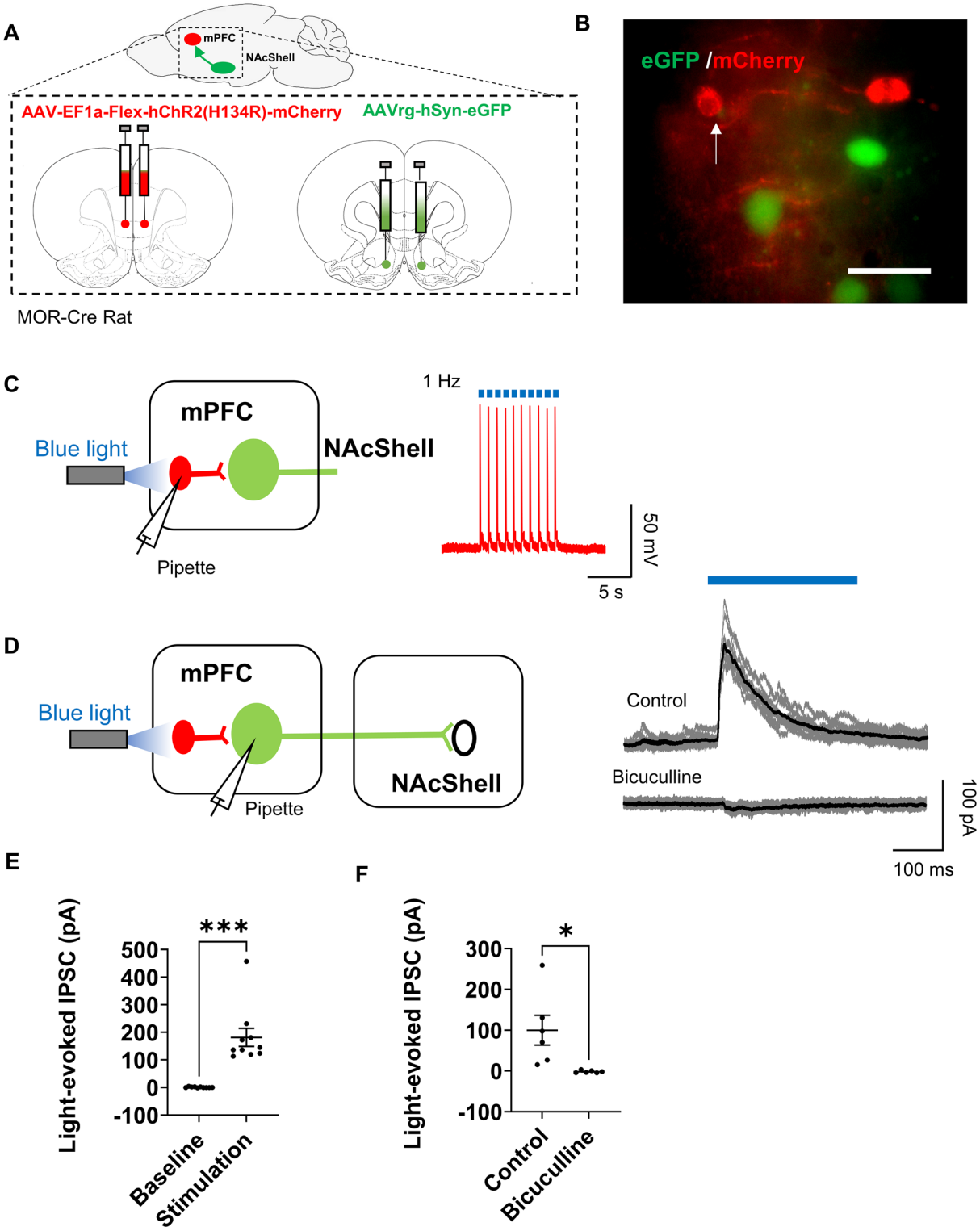

behavioural aspect of nicotine addiction, independent of the direct pharmacological effect of nicotine.

MOR$^+$ Neurons in the mPFC Inhibit Excitatory Projection to the NAcShell

MOR is dominantly expressed in GABAergic interneurons in layer 5 of the mPFC and regulates the excitatory outflow

◂**Fig. 5** MOR^+ neurons in layer 5 inhibit the mPFC-NAcShell circuit. **A** Diagram of the injection of AAVrg-hSyn-eGFP into the NAcShell and AAV-EF1a-Flex-hChR2(H134R)-mCherry into the mPFC of MOR-Cre rat. **B** The expression of eGFP (green) and ChR2-mCherry (red) in the mPFC neurons, scale bar, 50 μm. **C** Left: diagram of the whole-cell patch recording from MOR^+ neurons in the mPFC. Right: representative sample trace of action potential evoked by blue light (300 ms, 1 Hz). **D** Left: diagram of the whole-cell patch recording from $eGFP^+$ pyramidal neurons in the mPFC. Right: two sample traces show light-evoked IPSCs in the control (top) and under the presence of 100 μmol/L bicuculline (bottom). **E** The amplitude of light-evoked IPSC on $eGFP^+$ pyramidal neurons ($n=10$). **F** The effect of 100 μmol/L bicuculline on the amplitude of light-evoked IPSC in the $eGFP^+$ pyramidal neurons ($n=10$). Paired *t*-test (the mean ± SEM. $*P<0.05$, $***P<0.001$). eGFP, enhanced green fluorescent protein; GABA, gamma-aminobutyric acid; IPSC, inhibitory postsynaptic current; mPFC, medial prefrontal cortex; NAcShell, shell of nucleus accumbens

of the mPFC [41, 42]. Thus, we finally investigated whether and how MOR^+ neurons in the mPFC directly regulate the activity of the mPFC-NAcShell circuit that was confirmed to be involved in nicotine-associated behavioural preference by using whole-cell patch-clamp recording in PFC brain slices. We concomitantly injected AAVrg-hSyn-eGFP into the NAcShell, and AAV-EF1a-Flex-hChR2(H134R)-mCherry into the mPFC of MOR-Cre rats (Fig. 5A). Two weeks after injection, mCherry-labelled MOR^+ neurons and eGFP-labelled pyramidal neurons were found in layer 5 of the mPFC (Fig. 5B). To confirm whether ChR2-expressing MOR neurons directly respond to light stimulation, we performed current-clamp recording on $mCherry^+$ neurons and applied blue light on the mPFC region (300 ms, 1 Hz). Light stimuli evoked action potential successfully, and it was completely reproduced on MOR^+ neurons (Fig. 5C). We then performed voltage-clamp recording on $eGFP^+$ neurons which project into the NAcShell. Blue light stimuli evoked the transient inhibitory postsynaptic current (IPSCs) at the holding of +10 mV, and these were completely blocked by 100 μmol/L bicuculline, a $GABA_A$ receptor antagonist (Fig. 5D–F). These data indicate that MOR^+ neurons in the mPFC inhibit NAcShell-projecting pyramidal neurons *via* $GABA_A$ receptors.

Discussion

The present study demonstrates the critical role of MOR^+ neurons in mPFC for the first time in regulating the behavioural aspect of nicotine addiction by disinhibiting the mPFC-NAcShell circuit. Here we provide a line of evidence that (1) the nicotine-associated behavioural preference was increased after nicotine conditioning, (2) brain-wide voxel-based statistical analysis revealed that the regional brain activity was significantly increased in the mPFC and correlated with nicotine-associated behavioural preference, (3) either the chemogenetic activation of MOR^+ neurons in the mPFC or suppression of the mPFC-NAcShell circuit abolished the formation and retention of the nicotine-associated behavioural preference, and (4) the MOR^+ neurons in the mPFC directly inhibited layer 5 pyramidal neurons that project into the NAcShell through $GABA_A$ receptors. Intensive efforts have been made over the past decades to investigate nicotine substance dependence which is mainly induced by the pharmacological effects of nicotine. Nicotine acts on nAChRs, which are abundantly expressed in the posterior ventral tegmental area (VTA) dopaminergic neurons and their presynaptic terminals in the NAc, to facilitate dopamine release in the NAc, which induces reward and reinforces nicotine-sustained intake [43]. Likewise, since the homomeric α7 nAChRs expressed in the presynaptic terminal of excitatory glutamatergic input to the VTA dopaminergic neurons, the increased excitatory glutamatergic input from the prefrontal cortical area to the VTA dopaminergic neurons have been implicated as a critical step in initiating nicotine substance dependence. In contrast, nicotine addiction is reinforced by smoking-related cues without the direct pharmacological effect of nicotine. Smoking-related cues, such as conditioned habits or specific scenes, have been considered a major reason for failure of cessation and high rates of relapse [44, 45]. In the present study, we successfully established nicotine-associated behavioural preference using the CPP paradigm and demonstrated that specific manipulation of MOR^+ neurons in the mPFC or the mPFC-NAcShell circuit modulates the nicotine-associated behavioural preference, independent of the direct pharmacological effect of nicotine. These results suggest that endogenous μ-opioid signals in the mPFC modulate excitatory outflow to the NAcShell, resulting in the formation and retention of the behavioural aspect of nicotine addiction.

The mPFC is a key structure that plays a critical role in emotional, cognitive, and executive functions [46] and is known to be involved in behaviour dependence such as gambling and binge disorders. Subjects with gambling disorders show increased prefrontal cortex activity, as measured by functional magnetic resonance imaging [47]. Patients with binge eating disorders also show activation of the ventral medial prefrontal cortex as measured by functional near-infrared spectroscopy [48]. Consistently, our small-animal neuroimaging analysis revealed that regional brain activity in the mPFC was significantly increased in response to nicotine-associated behavioural preference and was positively correlated with nicotine-associated behavioural preference (Fig. 2C). MORs are expressed in the mPFC and modulate the outflow of the mPFC which may contribute to addictive disorders by altering cognitive and executive functions [49]. MORs are predominantly expressed in inhibitory interneurons in layer 5 of the mPFC and directly modulate projection

pyramidal neurons *via* monosynaptic $GABA_A$ receptors [41, 50]. Consistently, we found that specific activation of the MOR^+ neurons in the mPFC inhibited nicotine-associated behavioural preference (Fig. 3D, J). Our whole-cell patch-clamp experiment also clearly demonstrated that the MOR^+ neurons in the mPFC directly inhibited the pyramidal neurons in layer 5 that projected into the NAcShell (Fig. 5D, E). Together with previous reports that endogenous opioids increased in the mPFC region in association with addictive disorders [51, 52], the present results suggested the crucial role of MOR^+ neurons in the mPFC modulating the excitatory outflow from the mPFC for the behavioural aspect of nicotine addiction.

We also found that excitatory outflow from the mPFC facilitated NAcShell activity, which may reinforce nicotine-associated behavioural preferences. The NAc receives dense projections from the mesolimbic dopaminergic system, such as the VTA, and is well known to be a key structure in the brain involved in reward processing and reinforcement [53, 54]. Several studies have demonstrated that the NAc plays a crucial role in substance dependence through the pharmacological effects of addictive substances, such as cocaine and heroin, which are known to facilitate dopamine transmission in the NAc [55, 56]. Recently, functional implications of the NAc have also been suggested in behavioural addiction without any direct stimulation from addictive substances, such as gambling disorders. In individuals with gambling disorders, the release of dopamine in the NAc reaches its maximum when performing a gambling task [57]. Hyper-neural activation of the NAc has also been observed by Fos expression in the early stages of binge eating in a rat model [58]. These observations suggest that the NAc may also interact with higher cognitive and executive functions, which are essential for the development and maintenance of behavioural addiction. The NAc receives intensive projections from the frontal cortex, including the mPFC [59] and interacts closely with these regions. Electrical stimulation of the mPFC results in phasic dopamine release in the NAc region [60]. The interaction between the mPFC and NAc is thought to be an underlying mechanism of some behavioural addictions. In the binge eating disorder model, neural firing rates in the mPFC and NAc significantly increased before and during palatable food consumption [61]. In patients with pathological gambling, the right ventral striatum shows increased functional connectivity with the mPFC [62]. Consistently, we found that chemogenetic inhibition of the mPFC-NAcShell circuit, either during or after nicotine conditioning, suppressed nicotine-associated behavioural preference without affecting nicotine-induced hyper-locomotor activity (Fig. 4D, J). These observations indicate that enhanced excitatory transmission from the mPFC to the NAcShell, modulated by endogenous opioid signals in the mPFC, may facilitate the reinforcement of nicotine-associated behavioural preference.

Interestingly, we found that the increased locomotor activity during the nicotine conditioning phase was not affected by chemogenetic manipulation of either MOR^+ neurons in the mPFC or the mPFC-NAcShell circuit (Figs 3H and 4H). Nicotine administration induces hyper-locomotor activity in rats [63]. The increase in locomotor activity is potentially partly through the nAChRs located in the VTA [64]. Consistent with this, we found that locomotor activity significantly increased in the control group during the conditioning phase immediately after nicotine injection (Fig. 3H, N, and Fig. 4H, N). Although chemogenetic manipulation of either MOR^+ neurons in the mPFC or the mPFC-NAcShell successfully inhibits nicotine-associated behavioural preference, the nicotine-induced hyper locomotor activity was not affected by such specific manipulation. These results suggest the regulatory role of MOR^+ neurons in the mPFC and its excitatory outflow to the NAcShell may be independent of the direct pharmacological effect of nicotine. Our brain-wide analysis also revealed that the regional brain activity in response to nicotine-associated behavioural preferences was completely different from the pharmacological effect of nicotine. As shown in Fig. S1, strong activation was observed in widespread thalamic regions, posterior cingulate cortex, VTA, and dorsal raphe, which mostly corresponded to nAChR distribution in the brain after nicotine injection. In contrast, regional brain activity related to the nicotine-associated behavioural preference was increased in the mPFC, dorsal medial striatum, and dorsal hippocampus and was mostly related to cognition, association, and spatial

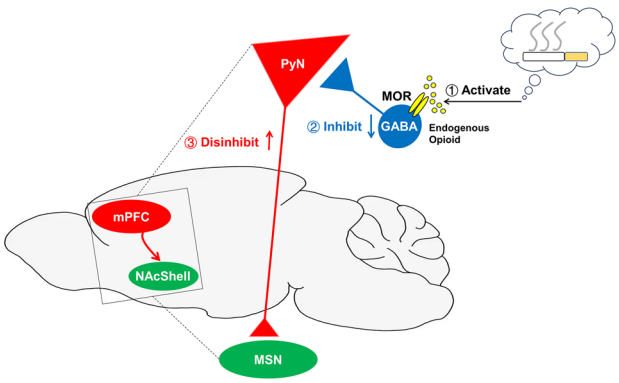

Fig. 6 Schematic displaying that MOR^+ neurons in the mPFC modulate excitatory outflow to the NAcShell to regulate the formation and retention of behavioural aspects of nicotine addiction. (1) The experience of nicotine-conditioning activates the MORs expressed in GABAergic interneurons in the mPFC region. (2) Activation of MORs inhibits the GABAergic interneurons. (3) Inhibition of MOR^+ interneurons results in the disinhibition of excitatory outflow from the mPFC to the NAcShell which contributes to the formation and retention of behavioural aspects of nicotine addiction. GABA, gamma-aminobutyric acid; PyN, pyramidal neuron; MOR, μ-opioid receptor; mPFC, medial prefrontal cortex; MSN, medium spiny neuron; NAcShell, shell of nucleus accumbens

learning. These results further support our hypothesis that endogenous opioid signals in the mPFC enhance the excitatory innervation of the NAcShell to drive the reinforcement of nicotine-associated behavioural preferences independent of the pharmacological effect of nicotine.

Our study demonstrated the activation pattern of the behavioural aspect of nicotine addiction. However, we did not conduct an experiment on nicotine substance dependence, such as the two-bottle choice. Chronic oral nicotine exposure usually lasts for several months and includes nicotine intake, preference, withdrawal, and escalation of nicotine consumption [65]. Our CPP paradigm only comprised triple nicotine injections but still successfully induced preference change. Therefore, we assumed that the existence of environmental cues could accelerate the process of nicotine behavioural dependence, in which the MORs and the mPFC-NAcShell circuits participate. Even though we demonstrated that MOR^+ neurons inhibit the mPFC-NAcShell circuit through $GABA_A$ receptors, there is still a limitation in our study that several other receptors also mediate the inhibitory neurotransmission [66], such as $GABA_B$ receptors and glycine receptors. More detailed investigations are needed to confirm whether and how these receptors are involved in nicotine-associated behavioural preference in the future.

In conclusion, our study demonstrated for the first time that MOR^+ neurons in the mPFC modulate excitatory outflow to the NAcShell to regulate the formation and retention of the behavioural aspect of nicotine addiction (Fig. 6). Most current intervention clinical trials have shown limited effects on smoking cessation and are mainly based on the pharmacological effects of nicotine. The main reasons for the failure of smoking cessation are attributed to smoking-conditioned habits and environmental cues which lead to nicotine reinforcement and relapse. In the present study, we demonstrated the novel molecular and neuronal mechanisms underlying the behavioural aspect of nicotine addiction which provide new insights for aiding smoking cessation.

Acknowledgements We thank Editage for manuscript editing help. This work was supported by JSPS KAKENHI (24659574, 26112003, and 15K14328), and JP 16H06276 (AdAMS).

Conflict of interest The authors declare no competing interests.

References

1. Mishra S, Mishra MB. Tobacco: Its historical, cultural, oral, and periodontal health association. J Int Soc Prev Community Dent 2013, 3: 12–18.
2. Le Foll B, Piper ME, Fowler CD, Tonstad S, Bierut L, Lu L. Tobacco and nicotine use. Nat Rev Dis Primers 2022, 8: 19.
3. Benowitz NL. Pharmacology of nicotine: Addiction, smoking-induced disease, and therapeutics. Annu Rev Pharmacol Toxicol 2009, 49: 57–71.
4. Tamburin S, Dal Lago D, Armani F, Turatti M, Saccà R, Campagnari S, *et al*. Smoking-related cue reactivity in a virtual reality setting: Association between craving and EEG measures. Psychopharmacology 2021, 238: 1363–1371.
5. Shiffman S, Dunbar M, Kirchner T, Li X, Tindle H, Anderson S, *et al*. Smoker reactivity to cues: Effects on craving and on smoking behavior. J Abnorm Psychol 2013, 122: 264–280.
6. Conklin CA, Coffman BA, McClernon FJ, Joyce C. Smokers' self-report and behavioral reactivity to combined personal smoking cues (proximal + environment + people): A pilot study. Brain Sci 2022, 12: 1547.
7. Spagnolo PA, Gómez Pérez LJ, Terraneo A, Gallimberti L, Bonci A. Neural correlates of cue- and stress-induced craving in gambling disorders: Implications for transcranial magnetic stimulation interventions. Eur J Neurosci 2019, 50: 2370–2383.
8. Limbrick-Oldfield EH, Mick I, Cocks RE, McGonigle J, Sharman SP, Goldstone AP, *et al*. Neural substrates of cue reactivity and craving in gambling disorder. Transl Psychiatry 2017, 7: e992.
9. Arend AK, Schnepper R, Lutz APC, Eichin KN, Blechert J. Prone to food in bad mood-Emotion-potentiated food-cue reactivity in patients with binge-eating disorder. Int J Eat Disord 2022, 55: 564–569.
10. Janes AC, Farmer S, Frederick BD, Nickerson LD, Lukas SE. An increase in tobacco craving is associated with enhanced medial prefrontal cortex network coupling. PLoS One 2014, 9: e88228.
11. Hayashi T, Ko JH, Strafella AP, Dagher A. Dorsolateral prefrontal and orbitofrontal cortex interactions during self-control of cigarette craving. Proc Natl Acad Sci U S A 2013, 110: 4422–4427.
12. Kober H, Mende-Siedlecki P, Kross EF, Weber J, Mischel W, Hart CL, *et al*. Prefrontal-striatal pathway underlies cognitive regulation of craving. Proc Natl Acad Sci U S A 2010, 107: 14811–14816.
13. Sun N, Laviolette SR, Addiction Research Group. Dopamine receptor blockade modulates the rewarding and aversive properties of nicotine via dissociable neuronal activity patterns in the nucleus accumbens. Neuropsychopharmacology 2014, 39: 2799–2815.
14. Xia L, Nygard SK, Sobczak GG, Hourguettes NJ, Bruchas MR. Dorsal-CA1 hippocampal neuronal ensembles encode nicotine-reward contextual associations. Cell Rep 2017, 19: 2143–2156.
15. Nygard SK, Hourguettes NJ, Sobczak GG, Carlezon WA, Bruchas MR. Stress-induced reinstatement of nicotine preference requires dynorphin/kappa opioid activity in the basolateral amygdala. J Neurosci 2016, 36: 9937–9948.
16. Xue YX, Chen YY, Zhang LB, Zhang LQ, Huang GD, Sun SC, *et al*. Selective inhibition of amygdala neuronal ensembles encoding nicotine-associated memories inhibits nicotine preference and relapse. Biol Psychiatry 2017, 82: 781–793.
17. Hillhouse TM, Olson KM, Hallahan JE, Rysztak LG, Sears BF, Meurice C, *et al*. The buprenorphine analogue BU10119 attenuates drug-primed and stress-induced cocaine reinstatement in mice. J Pharmacol Exp Ther 2021, 378: 287–299.
18. De Sa Nogueira D, Bourdy R, Filliol D, Romieu P, Befort K. Hippocampal mu opioid receptors are modulated following cocaine self-administration in rat. Eur J Neurosci 2021, 53: 3341–3349.
19. Brown TG, Xu J, Hurd YL, Pan YX. Dysregulated expression of the alternatively spliced variant mRNAs of the mu opioid receptor gene, OPRM1, in the medial prefrontal cortex of male human heroin abusers and heroin self-administering male rats. J Neurosci Res 2022, 100: 35–47.
20. Tanda G, Di Chiara G. A dopamine-mu1 opioid link in the rat ventral tegmentum shared by palatable food (Fonzies) and non-psychostimulant drugs of abuse. Eur J Neurosci 1998, 10: 1179–1187.
21. Krause D, Warnecke M, Schuetz CG, Soyka M, Manz KM, Proebstl L, *et al*. The impact of the opioid antagonist naloxone on experimentally induced craving in nicotine-dependent individuals. Eur Addict Res 2018, 24: 255–265.

22. King AC, Meyer PJ. Naltrexone alteration of acute smoking response in nicotine-dependent subjects. Pharmacol Biochem Behav 2000, 66: 563–572.
23. Hutchison KE, Monti PM, Rohsenow DJ, Swift RM, Colby SM, Gnys M, *et al*. Effects of naltrexone with nicotine replacement on smoking cue reactivity: Preliminary results. Psychopharmacology 1999, 142: 139–143.
24. Cui Y, Toyoda H, Sako T, Onoe K, Hayashinaka E, Wada Y, *et al*. A voxel-based analysis of brain activity in high-order trigeminal pathway in the rat induced by cortical spreading depression. Neuroimage 2015, 108: 17–22.
25. Zeng Y, Hu D, Yang W, Hayashinaka E, Wada Y, Watanabe Y, *et al*. A voxel-based analysis of neurobiological mechanisms in placebo analgesia in rats. Neuroimage 2018, 178: 602–612.
26. Cui Y, Neyama H, Hu D, Huang T, Hayashinaka E, Wada Y, *et al*. FDG PET imaging of the pain matrix in neuropathic pain model rats. Biomedicines 2022, 11: 63.
27. Schweinhardt P, Fransson P, Olson L, Spenger C, Andersson JLR. A template for spatial normalisation of MR images of the rat brain. J Neurosci Methods 2003, 129: 105–113.
28. Neyama H, Wu Y, Nakaya Y, Kato S, Shimizu T, Tahara T, *et al*. Opioidergic activation of descending pain inhibitory system underlies placebo analgesia. bioRxiv 2023. DOI:https://doi.org/10.1101/2023.06.26.546410.
29. Kilkenny C, Browne WJ, Cuthill IC, Emerson M, Altman DG. Improving bioscience research reporting: The ARRIVE guidelines for reporting animal research. PLoS Biol 2010, 8: e1000412.
30. Natarajan R, Wright JW, Harding JW. Nicotine-induced conditioned place preference in adolescent rats. Pharmacol Biochem Behav 2011, 99: 519–523.
31. Xu W, He Y, Zhang J, Li H, Wan X, Li M, *et al*. Simvastatin blocks reinstatement of cocaine-induced conditioned place preference in male mice with brain lipidome remodeling. Neurosci Bull 2021, 37: 1683–1702.
32. Schmill MP, Cadney MD, Thompson Z, Hiramatsu L, Albuquerque RL, McNamara MP, *et al*. Conditioned place preference for cocaine and methylphenidate in female mice from lines selectively bred for high voluntary wheel-running behavior. Genes Brain Behav 2021, 20: e12700.
33. McKendrick G, Graziane NM. Drug-induced conditioned place preference and its practical use in substance use disorder research. Front Behav Neurosci 2020, 14: 582147.
34. Huang T, Okauchi T, Hu D, Shigeta M, Wu Y, Wada Y, *et al*. Pain matrix shift in the rat brain following persistent colonic inflammation revealed by voxel-based statistical analysis. Mol Pain 2019, 15: 1744806919891327.
35. Marks MJ, Burch JB, Collins AC. Genetics of nicotine response in four inbred strains of mice. J Pharmacol Exp Ther 1983, 226: 291–302.
36. Ksir C, Hakan RL, Kellar KJ. Chronic nicotine and locomotor activity: Influences of exposure dose and test dose. Psychopharmacology 1987, 92: 25–29.
37. Kiianmaa K, Tuomainen P, Makova N, Seppä T, Mikkola JA, Petteri Piepponen T, *et al*. The effects of nicotine on locomotor activity and dopamine overflow in the alcohol-preferring AA and alcohol-avoiding ANA rats. Eur J Pharmacol 2000, 407: 293–302.
38. Kuwabara H, Heishman SJ, Brasic JR, Contoreggi C, Cascella N, Mackowick KM, *et al*. Mu opioid receptor binding correlates with nicotine dependence and reward in smokers. PLoS One 2014, 9: e113694.
39. Hurley SW, Carelli RM. Activation of infralimbic to nucleus accumbens shell pathway suppresses conditioned aversion in male but not female rats. J Neurosci 2020, 40: 6888–6895.
40. Ikemoto S, Qin M, Liu ZH. Primary reinforcing effects of nicotine are triggered from multiple regions both inside and outside the ventral tegmental area. J Neurosci 2006, 26: 723–730.
41. Witkowski G, Szulczyk P. Opioid mu receptor activation inhibits sodium currents in prefrontal cortical neurons via a protein kinase A- and C-dependent mechanism. Brain Res 2006, 1094: 92–106.
42. Férézou I, Hill EL, Cauli B, Gibelin N, Kaneko T, Rossier J, *et al*. Extensive overlap of mu-opioid and nicotinic sensitivity in cortical interneurons. Cereb Cortex 2007, 17: 1948–1957.
43. Wills L, Ables JL, Braunscheidel KM, Caligiuri SPB, Elayouby KS, Fillinger C, *et al*. Neurobiological mechanisms of nicotine reward and aversion. Pharmacol Rev 2022, 74: 271–310.
44. Janes AC, Pizzagalli DA, Richardt S, de Frederick B, Chuzi S, Pachas G, *et al*. Brain reactivity to smoking cues prior to smoking cessation predicts ability to maintain tobacco abstinence. Biol Psychiatry 2010, 67: 722–729.
45. Field M, Marhe R, Franken IHA. The clinical relevance of attentional bias in substance use disorders. CNS Spectr 2014, 19: 225–230.
46. Zheng J, Liu N, Xu H. Pathway matters: Prefrontal control of negative emotions *via* distinct downstream regions. Neurosci Bull 2022, 38: 226–228.
47. Tanabe J, Thompson L, Claus E, Dalwani M, Hutchison K, Banich MT. Prefrontal cortex activity is reduced in gambling and nongambling substance users during decision-making. Hum Brain Mapp 2007, 28: 1276–1286.
48. Veit R, Schag K, Schopf E, Borutta M, Kreutzer J, Ehlis AC, *et al*. Diminished prefrontal cortex activation in patients with binge eating disorder associates with trait impulsivity and improves after impulsivity-focused treatment based on a randomized controlled IMPULS trial. Neuroimage Clin 2021, 30: 102679.
49. Melugin PR, Nolan SO, Siciliano CA. Bidirectional causality between addiction and cognitive deficits. Int Rev Neurobiol 2021, 157: 371–407.
50. Baldo BA. Prefrontal cortical opioids and dysregulated motivation: A network hypothesis. Trends Neurosci 2016, 39: 366–377.
51. Yoo JH, Kitchen I, Bailey A. The endogenous opioid system in cocaine addiction: What lessons have opioid peptide and receptor knockout mice taught us? Br J Pharmacol 2012, 166: 1993–2014.
52. Gorelick DA, Kim YK, Bencherif B, Boyd SJ, Nelson R, Copersino M, *et al*. Imaging brain mu-opioid receptors in abstinent cocaine users: Time course and relation to cocaine craving. Biol Psychiatry 2005, 57: 1573–1582.
53. Hikida T, Morita M, MacPherson T. Neural mechanisms of the nucleus accumbens circuit in reward and aversive learning. Neurosci Res 2016, 108: 1–5.
54. Floresco SB. The nucleus accumbens: An interface between cognition, emotion, and action. Annu Rev Psychol 2015, 66: 25–52.
55. Corre J, van Zessen R, Loureiro M, Patriarchi T, Tian L, Pascoli V, *et al*. Dopamine neurons projecting to medial shell of the nucleus accumbens drive heroin reinforcement. Elife 2018, 7: e39945.
56. Kiyatkin EA, Stein EA. Fluctuations in nucleus accumbens dopamine during cocaine self-administration behavior: An *in vivo* electrochemical study. Neuroscience 1995, 64: 599–617.
57. Linnet J, Mouridsen K, Peterson E, Møller A, Doudet DJ, Gjedde A. Striatal dopamine release codes uncertainty in pathological gambling. Psychiatry Res 2012, 204: 55–60.
58. Hildebrandt BA, Sinclair EB, Sisk CL, Klump KL. Exploring reward system responsivity in the nucleus accumbens across chronicity of binge eating in female rats. Int J Eat Disord 2018, 51: 989–993.
59. Tzschentke TM, Schmidt WJ. Functional relationship among medial prefrontal cortex, nucleus accumbens, and ventral tegmental area in locomotion and reward. Crit Rev Neurobiol 2000, 14: 131–142.

60. Hill DF, Parent KL, Atcherley CW, Cowen SL, Heien ML. Differential release of dopamine in the nucleus accumbens evoked by low-versus high-frequency medial prefrontal cortex stimulation. Brain Stimul 2018, 11: 426–434.
61. Quansah Amissah R, Basha D, Bukhtiyarova O, Timofeeva E, Timofeev I. Neuronal activities during palatable food consumption in the reward system of binge-like eating female rats. Physiol Behav 2021, 242: 113604.
62. Koehler S, Ovadia-Caro S, van der Meer E, Villringer A, Heinz A, Romanczuk-Seiferth N, *et al*. Increased functional connectivity between prefrontal cortex and reward system in pathological gambling. PLoS One 2013, 8: e84565.
63. Koehl M, Bjijou Y, Le Moal M, Cador M. Nicotine-induced locomotor activity is increased by preexposure of rats to prenatal stress. Brain Res 2000, 882: 196–200.
64. Reavill C, Stolerman IP. Locomotor activity in rats after administration of nicotinic agonists intracerebrally. Br J Pharmacol 1990, 99: 273–278.
65. Bagdas D, Diester, Riley J, Carper M, Alkhlaif Y, AlOmari D, *et al*. Assessing nicotine dependence using an oral nicotine free-choice paradigm in mice. Neuropharmacology 2019, 157: 107669.
66. Bowery NG, Smart TG. GABA and glycine as neurotransmitters: A brief history. Br J Pharmacol 2006, 147: S109–S119.